Reprinted from The Journal of Physical Chemistry, 1995, 99.

Folding Model Proteins Using Kinetic and Thermodynamic Annealing of the Classical Density Distribution

Patricia Amara and John E. Straub*

Department of Chemistry, Boston University, Boston, Massachusetts 02215

Received: March 17, 1995; In Final Form: June 2, 1995[⊗]

The folding of several model proteins is studied using three optimization algorithms which are based on the simulated annealing of an approximation to the classical density distribution. These methods are derived from the approximate solution of equations of motion for the time or temperature evolution of the density distribution. Therefore, it is of interest to analyze not only the resulting lowest energy molecular conformations but also the folding mechanism followed during the annealing runs. The results are compared with classical simulated annealing based on molecular dynamics and the diffusion equation method of Scheraga and co-workers. The model proteins studied are 22-mers and a 46-mer based on a three-letter code used by Honeycutt and Thirumalai. The potential models the basic properties of attractive interactions between hydrophobic residues, to encourage the formation of a hydrophobic core, and the propensity of hydrophilic residues to be found at the protein surface. Analysis of the thermodynamically dominant structures during annealing reveals a collapse transition at high temperature followed by a strong folding transition to the native state at lower temperatures. This general mechanism has been seen previously in simulations of similar model proteins and predicted on the basis of mean field theories of heteropolymers. We find that the probability of success in finding the set of lowest energy native states is strongly correlated with the energy separation between the native (and native-like) and non-native states. Our optimization algorithms are effective in finding those low-energy structures which correspond to the global energy minimum fold. The results indicate that dynamical phase space simulated annealing methods may have an advantage over configuration space based search for complex fold topologies.

I. Introduction

For many years the protein folding problems have been addressed as one of global optimization. Once it is assumed that the native folded state of a protein is the thermodynamically dominant free energy minimum, the problem of finding the native state is one of finding the conformation of the lowest free energy minimum of a given protein sequence.[1] If we further assume that at room temperature the lowest free energy compact state will also be the compact state of lowest enthalpy or energy, the protein folding problem is a global energy minimization problem. A variety of methods have been created to address this problem.[2,3] Some of the most promising algorithms for molecular global energy minimization emerged as an amalgam of the simulated annealing protocol[4] and a "smoothing" transformation of the potential energy surface.[3] While simulated annealing provides a general strategy for global optimization, for problems of molecular optimization, where there is a broad distribution of energy scales, a near optimal cooling schedule may be prohibitively expensive. Smoothing transformations provide a way to remove many of the troublesome local minima on the potential surface in addition to lowering energy barriers. In some algorithms, the annealing step takes the form of a simple steepest descent quench on the smoothed potential surface[5,6] while in others a kinetic[7] or thermodynamic[8] annealing is performed.

Recently, a convergent evolution of ideas regarding the kinetics and thermodynamics of protein folding has emerged from detailed theoretical and simulation studies of "minimal" protein models. The general features were first recognized in theoretical models[9-11] and seen in simulation studies of model proteins both on and off lattice.[12-19] It has been proposed that folding occurs as a process of (1) on early collapse transition and (2) subsequent rearrangement within a set of compact states, (3) followed by a transition to the native state. The initial collapse transition, from a reduced or random coil state, dominant at high temperatures, to a compact state, occurs with a characteristic temperature T_θ and is similar to a homopolymer collapse transition.[16,20,21] It has been proposed that homopolymer collapse consists of two steps: (1) an early random collapse to a compact state followed by (2) slower reorganization to a lower energy compact state.[22,23] This is in agreement with the results of simulations of lattice[16] and continuous space models of homopolymers.[24] The radius of gyration is a good order parameter for the first stage of collapse, while the second state of rearrangement occurs largely within the set of compact states. During this collapse and rearrangement, only a fraction of the native character of the molecule is acquired. At lower temperature, there is a final folding transition to the native state which appears to be approximately first order with a characteristic transition temperature T_f.[9,15,25-27] In this transition most of the native state is acquired.[15] Wolynes and co-workers have discussed the significance of a possible intervening glass transition which implies a third characteristic temperature T_g,[9] and Shakhnovich and Gutin have discussed a related critical temperature T_c.[28]

Regarding kinetics, there is evidence that fast folding to the native state occurs for some trajectories via a nucleation pathway while other trajectories are trapped for some time in non-native conformations and must proceed via an activated transition over an energy barrier to the native state.[9,27,29] Regardless of the details, the behavior of these simple model proteins is rich and shares many of the characteristics of the folding of real proteins measured experimentally.[30]

[⊗] Abstract published in *Advance ACS Abstracts*, September 1, 1995.

0022-3654/95/2099-14840$09.00/0

In this paper, we present the results for the application of two global optimization algorithms to a series of model proteins. These proteins are based on a "minimal" model—a three-letter code proposed by Honeycutt and Thirumalai.[14] It has been shown[14,27,31] that these model proteins exhibit a rich thermodynamic and kinetic behavior which shares many similarities with lattice models and experimental studies of real proteins. We demonstrate the effectiveness of our optimization algorithms and offer a detailed comparison of the properties of (1) classical simulated annealing using molecular dynamics, kinetic annealing using a Gaussian phase space density distribution representation of an ensemble of protein conformations based on (2) Fokker–Planck[8] or (3) Smoluchowski dynamics,[32] (4) a thermodynamic annealing, directly in temperature, of a similar Gaussian configuration space distribution representation,[8] and (5) the diffusion equation method of Scheraga and co-workers.[6]

It has been observed that the mechanism followed during simulated annealing runs is often similar to the dynamics of a folding transition seen when the temperature is suddenly dropped below the folding temperature and the system relaxes to equilibrium.[27] Therefore, simulated annealing algorithms based on an exact or approximate dynamics may provide evidence for the kinetics of folding in addition to a distribution of low-energy final conformations. We interpret the detailed folding pathways generated during the optimization run in terms of the characteristic temperatures found in the original studies of the model system. Finally, the results are rationalized in terms of an effective annealing temperature, below which the annealing process is ineffective, and the features of the density of local potential energy minima.

II. Optimization Methods

In this section we define the algorithms employed in our study. Simulated annealing using molecular dynamics or Monte Carlo is one of the standards for global optimization of molecular systems,[4,33] and it is used throughout our study. We define a number of algorithms which follow the simulated annealing protocol for a coarse-grained classical dynamics. These algorithms differ from one another in terms of (1) being based on representations of the system in phase space or configuration space and (2) whether the annealing is dynamical, with a cooling schedule describing how the temperature is reduced in time, or carried out by direct integration in temperature. We also describe the diffusion equation method of Scheraga and co-workers which we apply in our study. The algorithms used here have been discussed elsewhere in detail.[3,7,8,32]

A. Gaussian Phase Packet Kinetic Annealing. In molecular dynamics simulation, a single conformation of an N-body system is represented by a point in the $6N$-dimensional phase space of positions and momenta. The dynamics of this point in phase space is given by Newton's equations of motion. In statistical mechanics an ensemble of conformations of a single system is represented by a continuous density distribution $\varrho(\mathbf{r},\mathbf{p},t)$ of positions, $\mathbf{r}$, and momenta, $\mathbf{p}$. The dynamics of the density distribution $\varrho(\mathbf{r},\mathbf{p},t)$ is described by the Liouville equation

$$\frac{\partial}{\partial t}\varrho(\mathbf{r},\mathbf{p},t) = -\mathcal{L}_0\varrho(\mathbf{r},\mathbf{p},t) \tag{1}$$

where $\mathcal{L}_0$ is the Liouville "streaming" operator

$$\mathcal{L}_0 = \frac{\mathbf{p}}{m}\nabla_{\mathbf{r}} + \mathbf{F}(\mathbf{r})\cdot\nabla_{\mathbf{p}} \tag{2}$$

The average of any property such as the potential $V(\mathbf{r})$ is

$$\langle V\rangle = \int \mathrm{d}^d\mathbf{r} \int \mathrm{d}^d\mathbf{p}\, \varrho(\mathbf{r},\mathbf{p},t)\, V(\mathbf{r}) \tag{3}$$

For a Gaussian density distribution the equations of motion are

$$\dot{\mathbf{r}}_0 = \mathbf{p}_0/m \qquad \dot{\mathbf{p}}_0 = -\nabla_{r_0}\langle V\rangle \tag{4}$$

$$\dot{M}_{2,0} = \frac{2}{m}M_{1,1} \qquad \dot{M}_{0,2} = -\frac{2}{d}M_{1,1}\nabla_{r_0}{}^2\langle V\rangle$$

$$\dot{M}_{1,1} = \frac{1}{m}M_{0,2} - \frac{1}{d}M_{2,0}\nabla_{r_0}{}^2\langle V\rangle$$

for the moments $\mathbf{r}_0 = \langle\mathbf{r}\rangle$, $\mathbf{p}_0 = \langle\mathbf{p}\rangle$, $M_{1,1} = \langle(\mathbf{r} - \mathbf{r}_0)(\mathbf{p} - \mathbf{p}_0)\rangle$, $M_{2,0} = \langle(\mathbf{r} - \mathbf{r}_0)^2\rangle$, and $M_{0,2} = \langle(\mathbf{p} - \mathbf{p}_0)^2\rangle$. As a result of the use of a spherical Gaussian single particle density, the equations of motion for the second-order moments, in general second rank tensors, are scalar.[32]

The center of the distribution follows Newton's equations on a fluctuating "coarse-grained" potential surface. Note that the classical equations for the density distribution allow "generalized tunneling" through barriers in that a packet may cross a barrier whose energy is higher than the fixed energy of the packet.

For purposes of simulated annealing, we need to control the temperature of the system. This can be done in a general way by coupling the system to a heat bath using the Fokker–Planck collision operator, for the phase space density distribution, or the Smoluchowski equation, for a reduced configuration space density distribution.[32,34] These algorithms are summarized below.

1. Fokker–Planck Packet Dynamics. The molecular dynamics of a system coupled to an external heat bath is often simulated using the Langevin equation. The bath influences the system dynamics through a friction, proportional to the momentum of the system particles, and a random force, which creates a balance in the system energy such that the average temperature of the system at equilibrium is the thermal energy k_BT.

The Langevin-based dynamics of a density distribution is described by the Fokker–Planck equation. The general form of the Liouville equation is

$$[\partial/\partial t + \mathcal{L}_0]\varrho(\mathbf{r},\mathbf{p},t) = -\mathcal{L}_c\varrho(\mathbf{r},\mathbf{p},t) \tag{5}$$

where $\mathcal{L}_c$ is the "collision" operator which introduces the effects of coupling to a heat bath. For the Fokker–Planck collision operator[35]

$$\mathcal{L}_c = -\gamma\nabla_{\mathbf{p}}\cdot[\mathbf{p} + mk_BT\nabla_{\mathbf{p}}] \tag{6}$$

the resulting equations of motion are[32]

$$\dot{\mathbf{r}}_0 = \mathbf{p}_0/m \qquad \dot{\mathbf{p}}_0 = -\nabla_{r_0}\langle V\rangle - \gamma\mathbf{p}_0 \tag{7}$$

$$\dot{M}_{2,0} = \frac{2}{m}M_{1,1}$$

$$\dot{M}_{1,1} = \frac{1}{m}M_{0,2} - \frac{1}{d}M_{2,0}\nabla_{r_0}{}^2\langle V\rangle - \gamma M_{1,1}$$

$$\dot{M}_{0,2} = -\frac{2}{d}M_{1,1}\nabla_{r_0}{}^2\langle V\rangle - 2\gamma[M_{0,2} - dmk_BT]$$

The centers relax by Langevin dynamics while the width of the momentum distribution is constrained about the correct temperature.

2. Smoluchowski Packet Dynamics. In the Fokker–Planck equation, when the system momenta relax quickly compared

to the positions, the dynamics is diffusive. It is then reasonable to estimate the inertial terms by assuming that the time derivative of the momentum is zero. This results in the adiabatic elimination of the velocities and the system may be completely described by the positions alone.

The dynamics of the reduced configurational space distribution function $\hat{\varrho}(\mathbf{r},t)$ is given by the Smoluchowski equation[34]

$$\frac{\partial}{\partial t}\hat{\varrho}(\mathbf{r},t) = \frac{1}{m\gamma}\nabla_{\mathbf{r}}\cdot[-\mathbf{F}(\mathbf{r}) + k_{\mathrm{B}}T\nabla_{\mathbf{r}}]\hat{\varrho}(\mathbf{r},t) \tag{8}$$

Employing a spherical Gaussian approximation to the configurational distribution

$$\hat{\varrho}(\mathbf{r},t) = (2\pi M_2/d)^{-d/2}\exp\left[-\frac{d}{2M_2}(\mathbf{r}-\mathbf{r}_0)^2\right] \tag{9}$$

the dynamics of the distribution are defined by the time dependence of the distribution center, $\mathbf{r}_0 = \langle\mathbf{r}\rangle$, and scalar variance, M_2. The equations of motion are[32]

$$\frac{\mathrm{d}\mathbf{r}_0}{\mathrm{d}t} = -\frac{1}{m\gamma}\nabla_{r_0}\langle V\rangle \qquad \frac{\mathrm{d}M_2}{\mathrm{d}t} = \frac{1}{m\gamma}\left[2dk_{\mathrm{B}}T - \frac{2}{d}M_2\nabla_{r_0}{}^2\langle V\rangle\right] \tag{10}$$

The equation of motion for the center of the density distribution is a steepest descent equation of motion on the coarse-grained effective potential $\langle V\rangle$. The value of M_2 adjusts to the curvature of the effective potential and will approach a static value when the delocalizing influence of the temperature balances the localizing influence of the potential.

B. Adiabatic Gaussian Density Annealing (aGDA) in Temperature. Systems for which the kinetic energy is solely a function of momentum, and the potential energy is solely a function of configuration, have a Hamiltonian of the form $H(\mathbf{r},\mathbf{p}) = T(\mathbf{p}) + V(\mathbf{r})$. In this very common case, the classical Bloch equation for the equilibrium density distribution ($\partial\varrho_{\mathrm{eq}}/\partial\beta = -H\varrho_{\mathrm{eq}}$) reduces to an equation of motion for the reduced configurational distribution function $\hat{\varrho}(\mathbf{r},\beta) = \exp(-\beta V(\mathbf{r}))/Z(\beta)$ where $Z(\beta) = \int \mathrm{d}\mathbf{r}\,\exp(-\beta V(\mathbf{r}))$ is the configurational integral in the canonical (constant N,V,T) ensemble. The reduced Bloch equation is simply

$$\frac{\partial}{\partial\beta}\hat{\varrho}(\mathbf{r},\beta) = -(V - \langle V\rangle)\hat{\varrho}(\mathbf{r},\beta) \tag{11}$$

which describes the temperature dependence of the equilibrium density distribution shared by the solution of the reduced form of the Bloch equation for the configurational distribution function. The mean field effective potential is defined as the average potential for the normalized density distribution $\hat{\varrho}(\mathbf{r},\beta)$

$$\langle V\rangle(\mathbf{r},\beta) = (2\pi M_2)^{-d/2}\int \mathrm{d}\mathbf{r}'\, V(\mathbf{r}')\mathrm{e}^{-d||\mathbf{r}-\mathbf{r}'||^2/2M_2} \tag{12}$$

To solve for the evolution of the equilibrium density distribution in β, we must choose a representation for $\hat{\varrho}(\mathbf{r},\beta)$ such as a Gaussian density distribution

$$\hat{\varrho}(\mathbf{r},\beta) = (2\pi M_2)^{-d/2}\exp\left[-\frac{d}{2M_2}(\mathbf{r}-\mathbf{r}_0)^2\right] \tag{13}$$

with center, $\mathbf{r}_0 = \langle\mathbf{r}\rangle$, and scalar variance, $M_2 = \langle(\mathbf{r}-\mathbf{r}_0)^2\rangle$ following the equations of motion in temperature

$$\frac{\mathrm{d}\mathbf{r}_0}{\mathrm{d}\beta} = -\frac{1}{d}M_2\nabla_{r_0}\langle V\rangle \tag{14}$$

$$\frac{\mathrm{d}M_2}{\mathrm{d}\beta} = -\frac{1}{d^2}M_2{}^2\nabla_{r_0}{}^2\langle V\rangle \tag{15}$$

$\langle V\rangle$ is the pair potential averaged over the distribution $\hat{\varrho}(\mathbf{r},\beta)$. These are the quantum mechanical imaginary time equations for $\hbar = 0$.[36]

We list several properties of these equations of motion and suggest the following protocol. (1) There is no cooling schedule. The method is defined completely by the initial conditions and a set of deterministic equations of motion in β. (2) The initial configuration must be chosen as the best guess at the solution which may, in practice, be a random configuration. The initial value of M_2 should be large (compared with the interparticle separation) to approximate the infinite temperature density distribution

$$\hat{\varrho}(\mathbf{r},\beta{=}0) \approx \text{constant} \tag{16}$$

(3) Guarantee that $\hat{\varrho}(\mathbf{r},\beta)$ is stationary

$$\dot{\mathbf{r}}_0 \propto \nabla_{r_0}\langle V\rangle = 0 \tag{17}$$

meaning there is no force on the distribution center.[37] (4) Update values of M_2 by integrating

$$\frac{\mathrm{d}M_2}{\mathrm{d}\beta} = -\frac{1}{d^2}M_2{}^2\nabla_{r_0}{}^2\langle V\rangle \tag{18}$$

for one step. Return to (3).

We have applied the original GDA algorithm (solving eq 14 and eq 15, simultaneously) and concluded that algorithms which allow centers to respond rapidly to changes in the M_2's are more effective as it was shown for applications involving Lennard-Jones clusters and water clusters in the work of Tsoo and Brooks[37] and discussed in detail elsewhere.[3]

C. The Diffusion Equation Method (DEM). Scheraga and co-workers have developed an optimization algorithm based on potential energy smoothing and local minimization. The DEM method has been applied to a range of conformational optimization problems including atomic clusters, water clusters, and small peptides. The DEM is based on a Gaussian coarse graining, or potential smoothing transformation, of the potential energy hypersurface defined as

$$\langle V\rangle_{\mathrm{DEM}}(\mathbf{r},t) = (4\pi Dt)^{-d/2}\int \mathrm{d}\mathbf{r}'\, V(\mathbf{r}')\mathrm{e}^{-||\mathbf{r}-\mathbf{r}'||^2/4Dt} \tag{19}$$

Interestingly, the effective potential in the GPP and aGDA algorithms, which results from an approximate coarse-grained classical dynamics, is identical to this transformed interaction potential.[6] The variance of the Gaussian is proportional to the diffusion "time" since $M_2 = 2dDt$.

To apply the algorithm, an initially large value of Dt is chosen. The particular value may be based on a convexity condition which shows the existence of a single minimum on the transformed potential surface at large enough Dt. The minimum (or minima) at the initial value of Dt is then found using a local minimizer. Dt is then gradually reduced while the minimum is followed continuously using a local minimization algorithm ending when $Dt = 0$. One way of understanding the DEM is to think of the aGDA algorithm for the special case that all M_2 values are identical.

III. Model Protein Potential and Integration Methods

For this study we employ a model protein potential developed by Honeycutt and Thirumalai[14] and similar to one used by Rey and Skolnick.[38] In this section, we describe the model potential and the integration schemes used for solving the various equations of motion discussed above. A detailed discussion of the effective potential $\langle V\rangle$ used in the density distribution based methods is given in the Appendix.

A. Averaged Effective Empirical Potentials for Proteins. When the N-body distribution is approximated as a product of

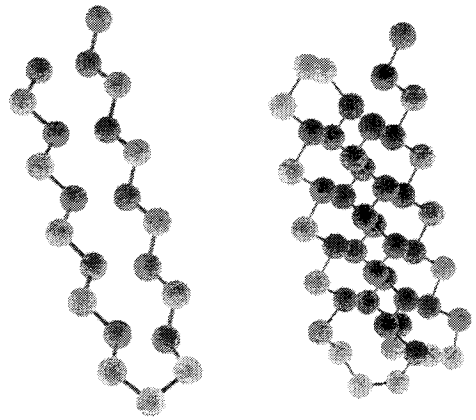

Figure 1. Ball and stick models of the lowest energy minimum conformation isolated in this study for the model proteins (a, left) the 22-mer $(LB)_5N_2(LB)_5$ and (b, right) the 46-mer $B_9N_3(LB)_4N_3B_9$ N_3-$(LB)_5L$.

spherically symmetric Gaussians,[39]

$$\varrho(\mathbf{r}^N,\mathbf{p}^N,t) = \prod_{k=1}^{N} \varrho_k(\mathbf{r}_k,\mathbf{p}_k,t) \tag{20}$$

it is straightforward to evaluate the effective potential for a pairwise additive potential energy function

$$\langle V\rangle = \sum_{i>j=1}^{N} \int d\mathbf{r}_i \int d\mathbf{p}_i \int d\mathbf{r}_j \int d\mathbf{p}_j \times \varrho_i(\mathbf{r}_i,\mathbf{p}_i)\, \varrho_j(\mathbf{r}_j,\mathbf{p}_j) V(|\mathbf{r}_i - \mathbf{r}_j|) \tag{21}$$

This can be rewritten

$$\langle V\rangle = \int_0^\infty dr\, G(r)\, V(r) \tag{22}$$

where the pair distribution function

$$G(r) = (\zeta/\pi)^{1/2} \frac{r}{r_{ij}} [\exp(-\zeta(r - r_{ij})^2) - \exp(-\zeta(r + r_{ij})^2)] \tag{23}$$

$r_{ij} = |\mathbf{r}_0^{(i)} - \mathbf{r}_0^{(j)}|$ and $\zeta = d/[2(M_{2,0}^{(i)} + M_{2,0}^{(j)})]$. The effective potential is easily evaluated when $V(\mathbf{r})$ is a Gaussian, exponential, or a polynomial.

The general form for the empirical potential function most popular in studies of proteins (CHARMM,[40] ECEPP[41]) is

$$V(r^N) = V_{\text{bond}} + V_{\text{angle}} + V_{\text{torsion}} + V_{\text{LJ}} + V_{\text{Coulomb}} \tag{24}$$

which includes bond, angle, and torsional contributions to the internal potential and Lennard-Jones and Coulombic nonbonded interactions. Using this form, it is natural to average each term over the many-body density distribution to calculate $\langle V\rangle$. We have done this and carried out extensive tests. We find that within the Gaussian density approximation, where the many-body density distribution is approximated by a product of single particle Gaussian distributions, an approximate form where the internal potential terms (bonds, angles, and torsions) act only on the packet centers is preferable. In that simplification, the effective potential is

$$\langle V\rangle = V_{\text{bond}} + V_{\text{angle}} + V_{\text{torsion}} + \langle V_{\text{LJ}}\rangle + \langle V_{\text{Coulomb}}\rangle \tag{25}$$

This potential was used throughout our study. In the dynamical equations of motion, the terms in brackets will contribute to the equations of motion for the centers and moments. The potential terms which depend *ad hoc* on the centers only (and are independent of the field variables $\mathbf{r}$ and $\mathbf{p}$) act only on the centers. The individual terms are discussed in the Appendix. Of course, any approximation in the construction of an optimization algorithm is valid if it can be justified empirically in terms of the effectiveness of the algorithm. The question is whether the dynamics remain valid. This point has been addressed elsewhere in the context of homopolymer collapse simulation[24] and will be discussed later in this work.

B. Three-Letter Code Models of Proteins. The model proteins studied here are based on the three-letter code of Honeycutt and Thirumalai[14] similar to a model of Rey and Skolnick[38] used in folding studies.[42] The three letters correspond to hydrophobic-type beads (B), hydrophilic-type beads (L), and neutral-type beads (N). The linear polymer is a chain of harmonic bonds

$$V_{\text{bond}}(\mathbf{r}) = (\kappa_b/2)(\mathbf{r} - \mathbf{r}_0)^2 \tag{26}$$

and angles

$$V_{\text{angle}}(\theta) = (\kappa_\theta/2)(\theta - \theta_0)^2 \tag{27}$$

where the equilibrium positions are $\mathbf{r}_0 = \sigma$ and $\theta_0 = 105°$ and the force constants are $\kappa_b = 400$ and $\kappa_\theta = 20$. The dihedral angle potential is

$$E_{\text{torsion}}(\phi) = A(1 + \cos[\phi]) + B(1 + \cos[3\phi]) \tag{28}$$

where the dihedral constants are defined to be $A = 0$ and $B = 0.2$ if two or more of the defining atoms i, j, k, and l are type N and $A = B = 1.2$ otherwise. With this parametrization, sequences running in repeating B and LB residues will tend to be rigid relative to areas near neutral N residues which are floppy and often act as turns. Therefore, because of the important role played by the dihedral potential, proteins designed using this three-letter code model may fold well.

The nonbonded potential is made of soft-sphere type repulsions and Lennard-Jones terms defined as

$$V_{\text{BB}}(r) = 4\epsilon[(\sigma/r)^{12} - (\sigma/r)^6]$$

$$V_{\text{LB,LL}}(r) = (8\epsilon/3)[(\sigma/r)^{12} + (\sigma/r)^6]$$

$$V_{\text{NN,NL,NB}}(r) = 4\epsilon(\sigma/r)^{12}$$

The V_{BB} potential is chosen to model the basic properties of attractive interactions between hydrophobic residues and to encourage the formation of a hydrophobic core. The repulsions between hydrophilic sites and all other residues model their tendency to be found at the protein surface. Therefore, the B and L residues are parametrized in a way that mimics the general properties of the statistically derived Sippl potential.[43] The neutral residues have a short-range repulsion when interacting with all other residues. These residues are modeled, primarily through the choice of dihedral potential, to form turns. In Figure 1 we display the lowest energy conformations found for the (a) 22-mer $(LB)_5N_2(LB)_5$, a β-turn, and (b) 46-mer $B_9N_3(LB)_4$-$N_3B_9N_3(LB)_5$ L, a β-turn sandwich, studied here.

C. MD Annealing and Leap-Frog Integration of GPP Based Equations. The equation of motion for advancing the positions in the annealing phase of the classical MD dynamics is taken to be

$$m\ddot{\mathbf{r}} = \mathbf{F} - \gamma\dot{\mathbf{r}} \tag{29}$$

where $\mathbf{F}$ includes the dihedral angle and the nonbonded interactions and γ determines the cooling rate. The equations

are integrated using a derivative of the Verlet algorithm

$$\mathbf{r}_{n+1} = \left(1 + \frac{\gamma h}{2m}\right)^{-1}\left[2\mathbf{r}_n - \left(1 - \frac{\gamma h}{2m}\right)\mathbf{r}_{n-1} + \frac{h^2}{m}\mathbf{F}_n\right]$$

where h is the time step and n is the iteration number. These equations lead to a near exponential reduction in the temperature during the run.

For the GPP equations of motion it is desirable to have a low-order integrator similar to the Verlet algorithm.[44] Recognizing that the equations of motion for $\dot{M}_{2,0}$ and $\dot{M}_{0,2}$ depend on $M_{1,1}$ only, and $\dot{M}_{1,1}$ is a function of $M_{2,0}$ and $M_{0,2}$, the equations of motion may be integrated using a generalization of the leap-frog algorithm[44] where $M_{2,0}$ and $M_{0,2}$ are updated on the time step with $\mathbf{r}_0$, while $M_{1,1}$ is updated with $\mathbf{p}_0$ on the half-step. For GPP constant energy dynamics or Fokker–Planck dynamics the leap-frog algorithm is defined on the time step

$$\mathbf{r}_0(t + \delta t) = \mathbf{r}_0(t) + \delta t\, \dot{\mathbf{r}}_0(t + \delta t/2)$$

$$M_{2,0}(t + \delta t) = M_{2,0}(t) + \delta t\, \dot{M}_{2,0}(t + \delta t/2)$$

$$M_{0,2}(t + \delta t) = M_{0,2}(t) + \delta t\, \dot{M}_{0,2}(t + \delta t/2) \qquad (30)$$

and on the half time step

$$\mathbf{p}_0(t + \delta t/2) = \mathbf{p}_0(t - \delta t/2) + \delta t\, \dot{\mathbf{p}}_0(t)$$

$$M_{1,1}(t + \delta t/2) = M_{1,1}(t - \delta t/2) + \delta t\, \dot{M}_{1,1}(t)$$

In certain equations, it might be necessary to provide a value of a moment one-half time step off the natural value. In that case, the algebraic mean of the bracketing time steps is substituted. These equations prove to be reasonably stable and significantly faster than algorithms such as the fourth-order Runge–Kutta method for the integration of the model protein dynamics.

IV. Results and Analysis

We have applied four algorithms to the folding of three model proteins based on the three-letter code of Honeycutt and Thirumalai.[14] In this section we discuss the results in terms of (1) the apparent "optimization pathways" or mechanism followed for each method and (2) the statistics of finding a low or global energy minimum configuration. The mechanism as well as the statistics helps us to determine which algorithm is most effective for each model.

We begin with an analysis of the mechanism of folding during optimization. To carry out this analysis, we follow the progress of an annealing run in terms of the following quantities. (1) The average potential energy $\langle V \rangle$ which for classical MD is the potential energy of a given configuration and for the density distribution based methods represents the potential energy averaged over the distribution of configurations given by $\varrho(\mathbf{r},\mathbf{p})$. The collapse and folding transitions are evident as rapid decreases in the potential energy. (2) The radius of gyration R_g defined for the GPP dynamics as

$$R_g^2 = \frac{1}{N}\sum_{k=1}^{N}[(\mathbf{r}_0^{(k)} - \mathbf{r}_c)^2 + M_{2,0}^{(k)}] \qquad (31)$$

For classical MD, $M_{2,0} = 0$ and the usual definition for a single molecule is recovered. In the algorithms based on a Gaussian approximation to the density distribution, the width of the distribution makes a contribution to the total gyration radius. R_g is a good order parameter for the collapse transition from an extended, entropy dominated state to a compact, energy dominated state and also for late rearrangements or "reopenings" from a collapsed conformation. (3) The native tertiary contact correlator defined[27]

$$C(t) = \frac{1}{N_{nbc}}\sum_i \sum_{j \geq (i+3)} \Theta[\alpha\sigma - r_{ij}(t)]\Theta[\alpha\sigma - r_{ij}^0] \qquad (32)$$

in analogy to similar measures used in spin glass studies is used to measure the similarity between the structure of an instantaneous configuration, with pair distances r_{ij}, and the target (in our case the "native" state or global energy minimum conformation), with pair distances r_{ij}^0. In the GPP-based methods, the distances are taken to be the difference between the average positions of atomic sites averaged over the density distribution, e.g., $r_{ij} = \langle |\mathbf{r}_i - \mathbf{r}_j| \rangle$. We take $\alpha = 2.9$ while σ is the Lennard-Jones diameter characterizing the nonbonded potential. N_{nbc} is the number of nonbonded contacts present in the target conformation. For the 22-mer $N_{nbc} = 70$. Therefore, if two sites are within a distance $\alpha\sigma$ in the target conformation *and* in the instantaneous conformation, there is a contribution to the correlator; when the instantaneous conformation is the target conformation, the correlator is unity. This correlator is a particularly good order parameter for the late transition from a compact state to the global energy minimum.

Relative timings for each annealing method are 100, 81, 55, 43, and 23 for the FP, the Smoluchowski, the aGDA, the DEM, and the MD, respectively.

A. Kinetic Transitions in Annealing. The kinetic simulated annealing algorithms were applied using (1) a Langevin-based MD algorithm (see above) with a value of $\gamma = 0.075$ and (2) the Fokker–Planck-based GPP algorithm using $\gamma = 0.075$. The temperature of the bath in each case was set to $T = 2.5$ for an equilibration period of 50 time units and then switched to zero. The system then cooled at a rate determined by the friction constant. This protocol was followed for 100 trajectories whose initial conditions were evenly sampled from a long equilibrium MD trajectory of 5000 time units at $T = 2$. For each algorithm we used a weak boundary potential $V_{bound} = (\kappa/2)(\mathbf{r} - \mathbf{r}_{com})^2$ where κ was for the 22-mer 0.07 (DEM and aGDA) and 0.03 (dynamical annealing) and for the 46-mer 0.01 (MD, aGDA, FP) and $\mathbf{r}_{com}$ is the center-of-mass position.

1. GPP with Fokker–Planck Dynamics. The GPP dynamics was highly successful, locating the global energy minimum of the 22-mer model with a 98% probability. The initial dynamics at $T = 2.5$ leads to an extended conformation with a large gyration radius seen in Figure 2a. At $t = 50$ the bath temperature is dropped to zero, and the system is annealed. There is an initial rapid collapse leading to a very compact conformation at $t \simeq 75$. However, as the temperature and potential energy continue to decrease, the molecule clearly "reopens", leading to a significant increase in the R_g followed by rearrangement and collapse to a more compact state. At a time near $t = 105$ there is a small but sharp drop in the potential energy, reflected by a rise in the temperature (a latent heat). Running to longer times refines this compact state, which is the global energy minimum.

The contact correlator provides a more detailed picture of the late transition. In Figure 2b the correlator shows the initial collapse transition to a compact state reaching a value of approximately $C(t) \simeq 0.8$. The "reopening" causes the loss of native contacts (not reflected in any rise in potential energy) which are re-formed in the later rapid transition to the native state occurring between $95 < t < 105$. The contact correlator is an excellent order parameter for the late transition to the well-folded global energy minimum state. We also show the energy of the quenched instantaneous configurations during the run.

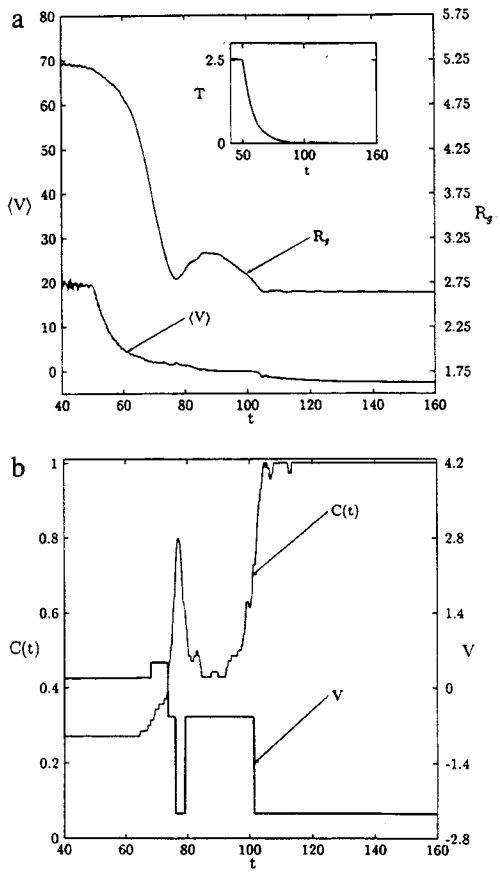

Figure 2. (a) Potential energy $\langle V \rangle$ and radius of gyration R_g are followed as a function of time t during the annealing for the model protein $(LB)_5N_2(LB)_5$ using the GPP Fokker–Planck algorithm. (b) Native tertiary contact correlator $C(t)$ measures the resemblance of an instantaneous structure to the native structure as it progresses during the annealing run using the GPP Fokker–Planck algorithm. The heavy line labeled V shows the energy of the instantaneous structure following local energy minimization.

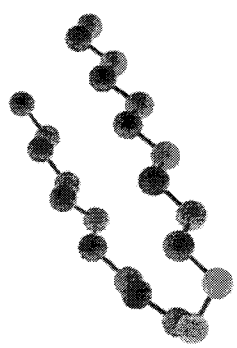

Figure 3. Ball-and-stick model of the intermediate quenched configuration for the 22-mer model protein $(LB)_5N_2(LB)_5$.

The peak in $C(t)$ coincides with the first visit to the global energy minimum basin. Following this visit, the molecule moves to a region of configuration space which drains to a local minimum (shown in Figure 3). Subsequently, there is a transition to the lower global energy minimum configuration correlated with a sharp transition in $C(t)$.

Analysis of the thermodynamics of annealing is based on an average of the 98 trajectories which folded to the global minimum binned by the instantaneous temperature. The results in Figure 4 indicate that the mechanism derived from the dynamics of a representative trajectory, a fast collapse to a compact but non-native state of low energy, followed by a

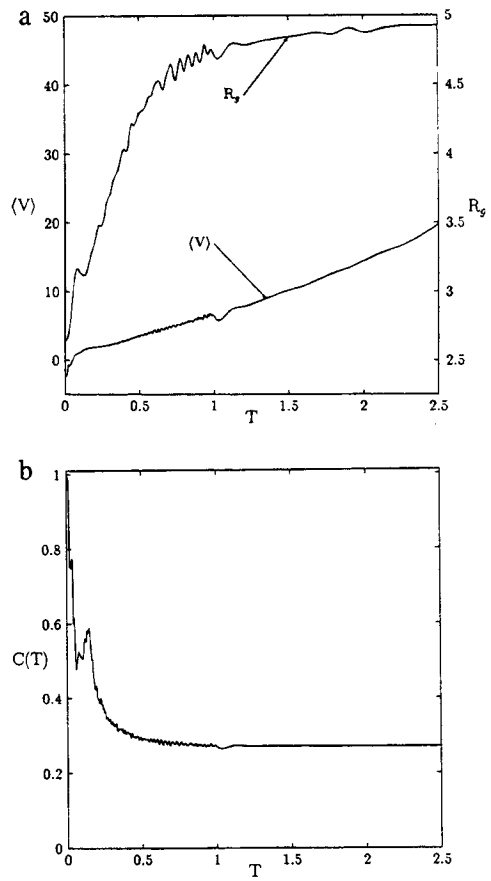

Figure 4. Averages for the 100 trajectories binned in temperature. (a) The potential energy $\langle V \rangle$ and radius of gyration R_g are followed as a function of temperature T during the annealing for the model protein $(LB)_5N_2(LB)_5$ using the GPP Fokker–Planck algorithm. (b) The native tertiary contact correlator $C(T)$ measures the resemblance of an instantaneous structure to the native structure as it progresses during the annealing run using the GPP Fokker–Planck algorithm.

reopening and rearrangement to the more compact global minimum state, is common for the GPP algorithm.

2. *Smoluchowski Dynamics.* The GPP-based Smoluchowski algorithm was applied with a value of $\gamma = 0.06$ and a temperature annealing schedule of $T(t) = 2.5 \exp(-\zeta t)$ and $\zeta = 0.075$. This protocol leads trajectories to the global energy minimum in 39% of the runs. The dynamics of the annealing is demonstrated in Figure 5a. The gyration radius shows a gradual decrease as the temperature is reduced. As the temperature is lowered, the collapse is gradual. The drop in the potential energy, which is more rapid, mirrors the decrease in temperature (see inset). Throughout the run, the average potential energy reduction is nearly linear in T as one would expect for an effectively harmonic system. In Figure 5b the contact correlator shows a more rapid rise to unity typical of the thermodynamic annealing algorithms.

3. *MD Annealing.* The MD simulated annealing, using the same cooling schedule and boundary potential as the GPP dynamics, was successful in finding the global energy minimum only 4% of the runs. The molecular dynamics annealing for the models discussed here has been described in the original work of Honeycutt and Thirumalai.[14] Figure 6a shows the dynamics of the energy and radius of gyration for a representative annealing run. The progression of R_g shows a clear collapse transition as the temperature is lowered. R_g is a good order parameter for this early transition. Since there is a single molecule, the average potential is noisy compared with the GPP

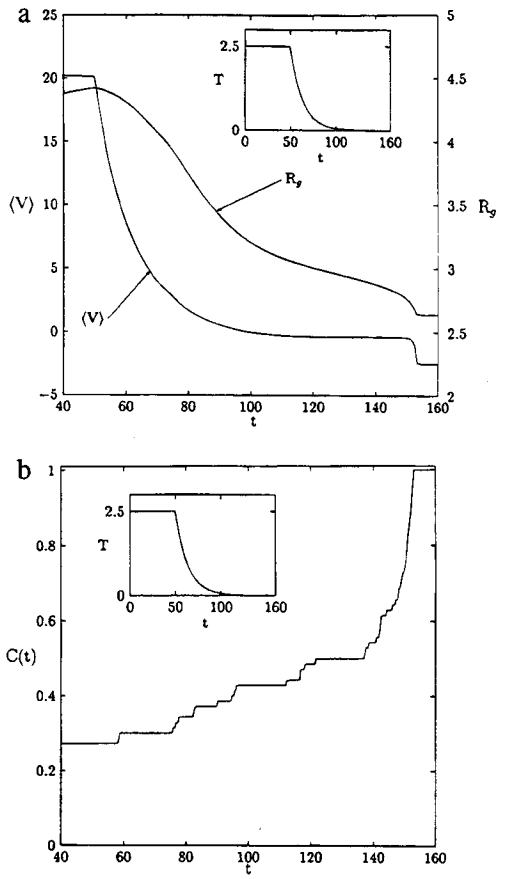

Figure 5. (a) Potential energy $\langle V \rangle$ and radius of gyration R_g are followed as a function of time t during the annealing for the model protein $(LB)_5N_2(LB)_5$ using the GPP Smoluchowski algorithm. (b) The native tertiary contact correlator $C(t)$ measures the resemblance of an instantaneous structure to the native structure as it progresses during the annealing run using the GPP Smoluchowski algorithm.

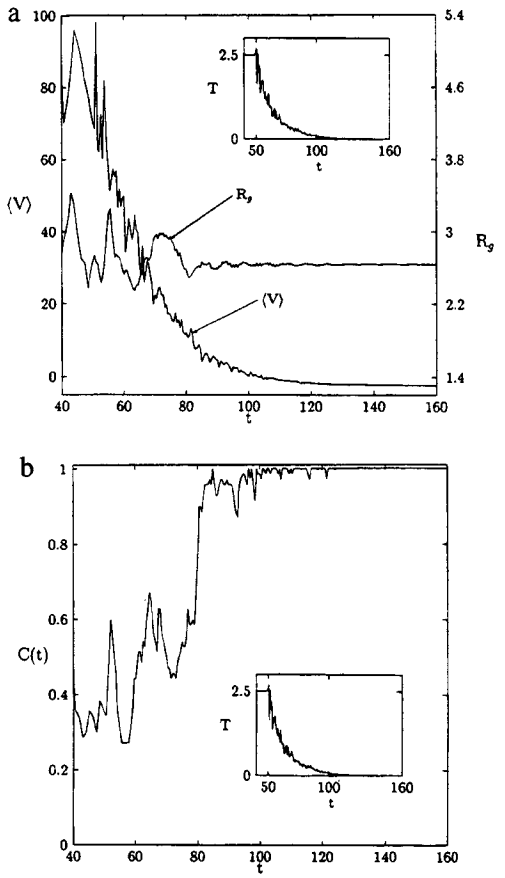

Figure 6. (a) Potential energy $\langle V \rangle$ and radius of gyration R_g are followed as a function of time t during the annealing for the model protein $(LB)_5N_2(LB)_5$ using the MD algorithm. (b) The native tertiary contact correlator $C(t)$ measures the resemblance of an instantaneous structure to the native structure as it progresses during the annealing run using the MD algorithm.

dynamics based on the time evolution of an approximate phase space density distribution.

Interestingly, there is a rise in R_g following the initial collapse as was seen in the GPP dynamics. Examining the contact correlator in Figure 6b, we see that the early collapse leads to a rise in the number of nativelike nonbonded contacts and the reopening, which leads to the increase in R_g, corresponds to a slight reduction in $C(t)$. Following the reopening, for $T < T_\theta$, the dynamics consists of rearrangements within a set of compact conformations as has been seen in the simulated dynamics of homopolymers.[24] However, unlike the case of homopolymers, at a lower temperature T_f there is a transition to a low or minimum energy compact state.

B. Thermodynamic Transitions in Annealing. The adiabatic GDA algorithm and the Smoluchowski dynamics algorithm were used to examine the characteristic thermodynamics for the 22-mer and 46-mer model proteins. The Smoluchowski dynamical equations were integrated using a Verlet algorithm. The aGDA equations were solved using a conjugate gradient algorithm to minimize the distribution center with fixed M_2 while the equation of motion for M_2 was updated with a fourth-order Runge−Kutta algorithm. The diffusion equation method was applied using a conjugate gradient algorithm. For each method, the initial value of $M_2 = 5$. These protocols were followed for 100 trajectories whose initial conditions were evenly sampled from a long equilibrium MD trajectory of 5000 time units at $T = 2$. For each algorithm we used a weak boundary potential $V_{bound} = (\kappa/2)(\mathbf{r} - \mathbf{r}_{com})^2$ where κ was varied from 0.02 to 0.2 and $\mathbf{r}_{com}$ is the center-of-mass position. This potential biased the annealing search toward the compact configurations and leads to higher probabilities of finding the global minimum with fast annealing schedules. Throughout the run, the boundary potential was a small fraction of the total energy. For the dynamics following the collapse transition the boundary potential was constant and did not contribute. Representative trajectories are analyzed here for the 22-mer and compared with the results of the DEM of Scheraga and coworkers.

1. Adiabatic Gaussian Density Annealing (aGDA). The first minimization of the center $\mathbf{r}_0$ of the density distribution maps all 100 initial configurations onto a single configuration. Therefore, there is a single trajectory for the aGDA algorithm, and that trajectory leads to the global energy minimum.

At high temperatures, the gyration radius $R_g \simeq 6.5$ and the molecule is fully extended as shown in Figure 7a. This is the expected conformation at high temperatures where entropy dominates the free energy. As the temperature is reduced, there is a gradual reduction in the average potential which leads to a sharp drop in R_g near $T = 1.0$. (We note here that the "temperature" of the aGDA algorithm is not simply related to a physical temperature in this study.) The subsequent collapse transition continues until the potential levels out. At a smaller value of the temperature there is a sharp drop in both R_g and $\langle V \rangle$ which corresponds to the density distribution localizing in the global energy minimum for the correct $T = 0$ distribution.

The contact correlator, displayed in Figure 7b, confirms the picture provided by the time dependence of R_g and $\langle V \rangle$ for the high-temperature collapse transition. $C(T)$ shows a significant

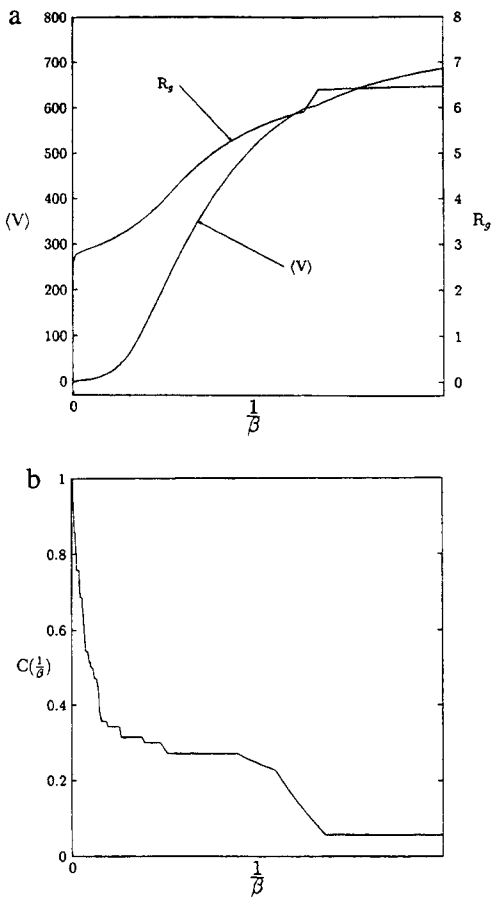

Figure 7. (a) Potential energy $\langle V \rangle$ and radius of gyration R_g are followed as a function of "temperature" $1/\beta$ during the annealing for the model protein $(LB)_5N_2(LB)_5$ using the aGDA algorithm. (b) The native tertiary contact correlator $C(T)$ measures the resemblance of an instantaneous structure to the native structure as it progresses during the annealing run using the aGDA algorithm.

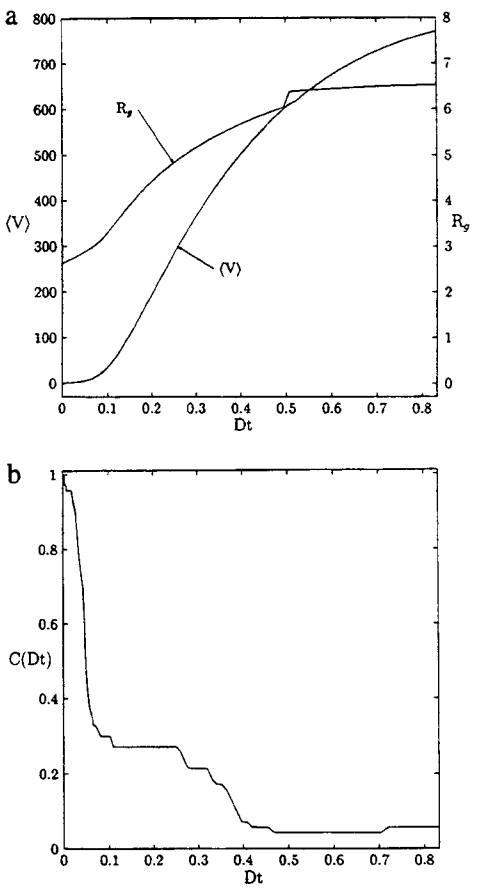

Figure 8. (a) Potential energy $\langle V \rangle$ and radius of gyration R_g are followed as a function of Dt during the annealing for the model protein $(LB)_5N_2(LB)_5$ using the diffusion equation method (DEM) algorithm. (b) The native tertiary contact correlator $C(Dt)$ measures the resemblance of an instantaneous structure to the native structure as it progresses during the annealing run using the DEM algorithm.

increase from the high-temperature limit, indicating that some of the native contacts of the target global energy minimum structure have been formed. As the temperature is lowered (integrating out to large β), there is a sharp transition near $T = 2$ during which the remaining 60% of the native contacts are formed. Clearly, $C(T)$ provides a more sensitive measure of the later localizing transition into the native state than the energy or gyration radius.

Therefore, while we cannot provide a physical temperature for these runs, we clearly see a process of collapse at high temperature and, at low enough temperature, a localization into the global minimum.

2. *Diffusion Equation Method.* The results of the DEM are shown in Figure 8. Clearly, the optimization "mechanism" of the DEM and aGDA algorithm is quite similar, as has been discussed in detail elsewhere.[8] The difference between the two algorithms is that in the DEM there is a single diffusion time (proportional to the site density distribution widths). Therefore, while the aGDA algorithm optimizes the value of M_2 for each site depending on the Laplacian of the average potential for that site, the DEM uses a single width for all sites. In the DEM algorithm the diffusion time is monotonically reduced while in the aGDA algorithm each site may fluctuate, increasing or decreasing, during the integration in β.

Nevertheless, the results are remarkably similar. In both cases, there is a single trajectory, and that trajectory leads to the global energy minimum for the 22-mer. The two transitions, most clearly depicted in Figures 7b and 8b, are quite similar. Therefore, in spite of the apparent differences in the algorithms, for the application to the 22-mer the results are practically identical.

C. Comparison of Results for Structural Optimization. The statistics for global optimization of the 22-mer model protein are shown in Figure 9. Clearly, the aGDA and DEM algorithms are most effective in the sense that each algorithm consists of a single trajectory run which leads to the global minimum conformation. However, the GPP-based dynamical annealing using the Fokker–Planck collisional coupling to a heat bath works nearly as well. Analysis of the trajectories shows that the dynamical annealing algorithms follow a number of separate pathways. Most trajectories collapse and then require a reopening before settling into the lower energy minimum. However, the aGDA and DEM algorithms follow a single pathway to the global minimum. The MD annealing is far less effective in finding low-energy minima for this model when held to the same annealing schedule as used by the GPP dynamical algorithms. While we say "single pathway" for the density distribution based methods, a broad distribution may indicate a variety of possible pathways.

We can compare the annealing methods by defining an effective annealing temperature T_{eff} from the best fit to $P^<(E)$ in Figure 9 using

$$P^<(E,T_{\text{eff}}) = \int_{-\infty}^{E} e^{-E'/k_B T_{\text{eff}}} g_\infty(E')\, dE' / \int_{-\infty}^{\infty} e^{-E'/k_B T_{\text{eff}}} g_\infty(E')\, dE' \quad (33)$$

Here $g_\infty(E)$ is the distribution of local minima energies taken

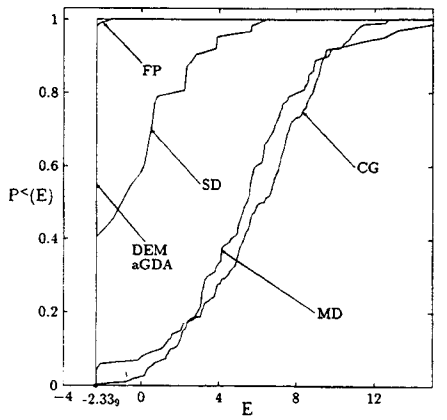

Figure 9. Global optimization of a 22-mer three-letter code model protein $(LB)_5N_2(LB)_5$ which folds to a global minimum of a single β-turn. Cumulative probability of finding a minimum with energy less than E, $P^<(E)$, for 100 runs using simulated annealing with conjugate gradient quench from high-temperature trajectories (CG), molecular dynamics (MD), Gaussian phase packets with Fokker–Planck (FP) or Smoluchowski (SD) dynamics, the adiabatic Gaussian density annealing (aGDA), and diffusion equation method (DEM) algorithms. The derivative of $P^<(E)$-labeled CG is defined as $g_\infty(E)$, meaning the distribution of local minima derived from deep quenches.

TABLE 1: Effective Annealing Temperature T_{eff} Defined as the Best Fit to the Form of $P^<(E)$ Using a Boltzmann-Weighted Average of the Distribution of Local Minima, Eq 33, Taken from a High-Temperature Quench of a Molecular Dynamics Run (See Figure 9)

	MD	Fokker–Planck	Smoluchowski	aGDA	DEM
T_{eff}	17.0	0.06	1.05	0.0	0.0

from a high-temperature quench of a molecular dynamics run. This means that effectively the equilibrium ensemble was well sampled for $T \geq T_{eff}$ but that below T_{eff} the molecule is glassy and is frozen in to a thermal distribution of minima at $T = T_{eff}$. Therefore, if $T_{eff} = \infty$, then the Boltzmann factor is unity and the distribution of minima found is the same as a quench from a high-temperature trajectory. There is no annealing. In the case of the aGDA or DEM algorithms applied to the 22-mer, all runs lead to the global energy minimum, and therefore $T_{eff} = 0$ which is the optimal result for an annealing run. The results for the algorithms studied in Figure 9 are shown in Table 1.

For the case of the GPP Smoluchowski dynamics the data for $P^<(E)$ are poorly fitted by the simple approximation in eq 33. It could be that this is due to the fact that the wells have unequal volumes (equal volumes are assumed in the approximate formula) and that the method itself is biased toward finding wells of larger volume (which survive the coarse graining) to an even greater extent due to the use of an approximate $\varrho(\mathbf{r},\beta)$.

The bounds on the variances of the packets for a single representative run are shown for the three packet annealing algorithms in Figure 10. The trends are quite similar to the behavior of the gyration radius for each method. Note that there is a dramatic early drop in the upper bound on the variances which is correlated with the collapse of the molecule. In the collapse, the curvature of the potential for each site is expected to be more positive and have a stronger localizing effect. The stronger transition in the lower bound at lower temperatures is correlated with the folding transition where the molecule's density distribution becomes localized to represent a single configuration.

For the 46-mer, MD annealing led 30% of the 10 trajectories to a low-energy native-like configuration while 50% were stranded at relatively high energies (more than 10 units above the native-like states) with values of the contact correlator which

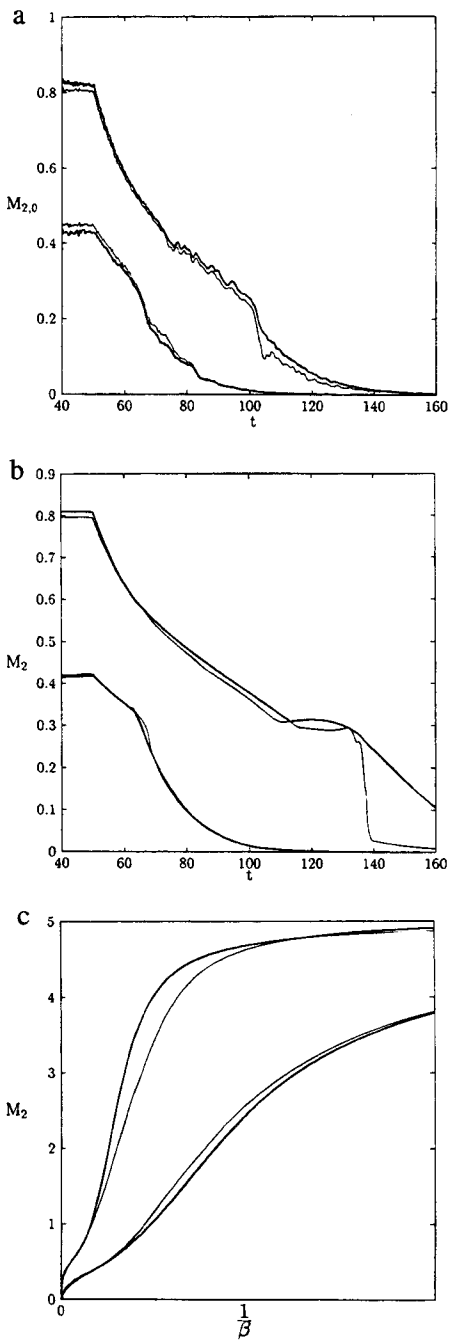

Figure 10. Bounds on the variances of the Gaussian packets for the average of the runs for the three methods: (a) GPP Fokker–Planck dynamical annealing, (b) GPP Smoluchowski dynamics, and (c) aGDA temperature annealing. The heavy upper and lower lines are the strict upper and lower bounds. Ten percent of the variances are found above, and 10% below, the lighter lines.

are below 0.7. This is in agreement with the earlier results on this model.[14] It is also a very interesting result. Apparently, for this larger model protein, MD annealing is more effective than for the case of the 22-mer. This will be discussed in more detail in the next section.

For the 46-mer, we find that the GPP annealing with the Fokker–Planck dynamics leads 30% of the trajectories to the basin containing the set of native-like states, if not to the lowest energy state among those native-like states. These native-like states have the correct β-sandwich fold but differ in having disorder in the loop regions. Another 60% of the trajectories found low-energy states which were not native-like in that one or more of the strands were in a very different orientation,

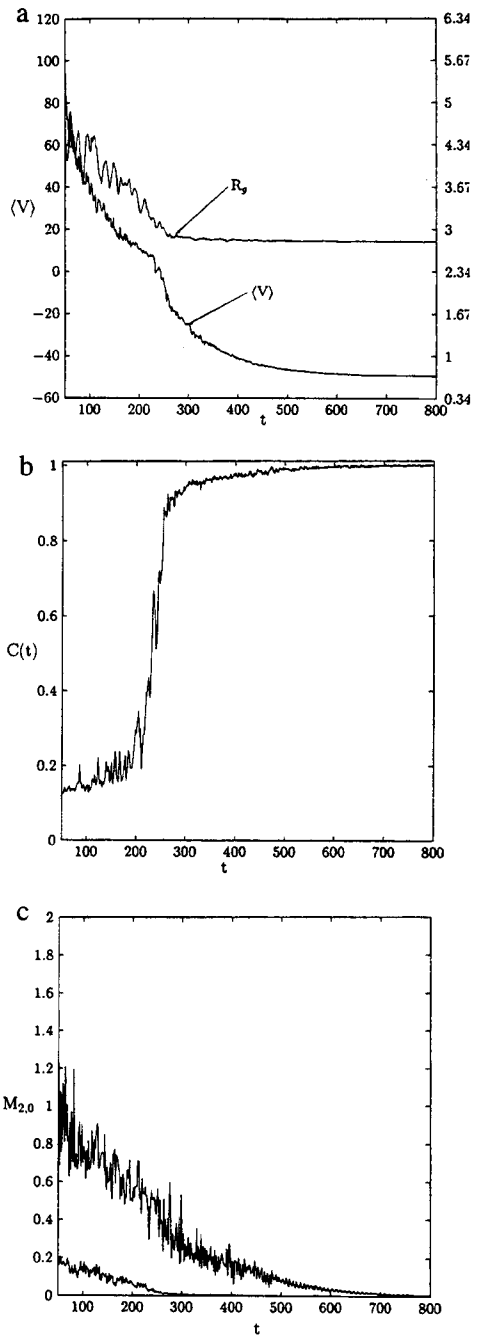

Figure 11. (a) Potential energy $\langle V \rangle$ and radius of gyration R_g are followed as a function of time t during the annealing for the model protein 46-mer $B_9N_3(LB)_4N_3B_9N_3(LB)_5$ L using the GPP-based Fokker–Planck algorithm. (b) The native tertiary contact correlator $C(t)$ measures the resemblance of an instantaneous structure to the native structure as it progresses during the annealing run. (c) The upper and lower bounds on the variances of the Gaussian packets.

breaking the β-sandwich fold. The lowest energy non-native fold was a near mirror image of the native state. For every Fokker–Planck annealing run, the contact correlator was eventually above 0.8 in contrast to the MD annealing. We feel that this is good result in that the practical goal of a folding algorithm should be to find a native-like substate with the correct fold and belonging to the set of substates sampled in equilibrium fluctuations at biological temperatures. The results for the correlator, average energy and gyration radius, and the upper and lower bounds on the packet variances are shown in Figure 11. Note that at early times and high temperatures the decrease in the gyration radius and potential energy is gradual and monotonic. After the time passes 200 there is a dramatic rise in the contact correlator $C(t)$ which coincides with the lower bound on the $M_{2,0}$'s dropping near zero and the gyration radius leveling off. After this transition, the potential energy appears to decrease exponentially while the correlator rises from just above 0.9 to unity. This decrease in the potential energy is well correlated with the decrease in the upper bound on the packet variances. The transition to the low-energy β-sandwich configuration in the 46-mer appears to be a single step, all-or-none transition. In the 22-mer folding, the process clearly involved two transitions. The transition for the 46-mer, using this particular cooling schedule, appears to combine the collapse and reorganization transitions into a single process, causing it to resemble the single-step mechanism as seen for a subset of trajectories in the study of this model.[27]

Interestingly, our results for the aGDA algorithm indicate that it, while perfectly effective for the 22-mer folding, has significant problems for the 46-mer where the fold topology is more complicated. For different initial values of M_2's, we tried to identify a boundary potential which would lead to the 100 initial configurations being mapped onto a single starting configuration following energy minimization (as for the 22-mer). However, for the boundary potentials examined, we obtained 100 distinct local minima. Starting from a fully extended configuration, the first minimization of the r_0's on the potential surface with fixed M_2's and with the boundary potential confining each particle to the center of mass, brought the polymer to a "U-shaped" configuration which then misfolded into a high-energy local minimum. In fact, we were unable to define a boundary condition which led to an initial configuration which mapped to a native-like state. This indicates that for a complicated fold the dynamical annealing algorithms, which allow for a more random search of conformational space, may have an advantage over the aGDA method in that the results are not as sensitive to the choice of boundary potential. If a boundary potential which annihilates the energy minimum corresponding to the native folded conformation on the smoothed potential is chosen, the aGDA algorithm may not explore that region of configuration space even though as the packets narrow that minimum emerges as the global minimum.[32,37,45] A dynamical annealing algorithm may begin in a basin corresponding to the wrong fold but may cross over a barrier on the smoothed potential once another conformation emerges as the lower energy minimum. This scenario is described in Figure 12.

D. Character of the Potential Energy Landscape. We can gain insight into the relative for success of the optimization algorithms in folding the model proteins studied here by examining the density of local minima for each model. We have carried out a long molecular dynamics trajectory of 5000 time units and quenched each of 100 evenly spaced instantaneous configurations to a nearby minimum using a conjugate gradient local minimization routine. This was carried out at three temperatures $T = 0.5$, 1.0, and 2.0. This analysis does not lead to exhaustive enumeration of the potential hypersurface's local minima. However, we found that additional runs did not qualitatively change the distribution, and aside from the knowledge of the few lowest energy minima, it is the qualitative features of the distribution that will be used in our analysis. Namely, extrapolating from the work of Honeycutt and Thirumalai on the 46-mer[14] and Karplus and Shakhnovich on lattice models,[18,19] we expect that sequences which fold will have a significant "energy gap" between the native (and native-like) and the non-native conformations.

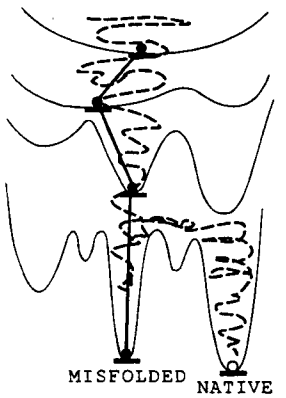

Figure 12. Schematic of the potential energy surface of a model protein is shown. The bottommost curve is the untransformed potential energy surface while other curves depict smoothed effective potential surfaces. In the uppermost curve the smoothing has annihilated all but one minimum on the surface. As the smoothing is lessened, local energy minima emerge, and eventually the unsmoothed, physical potential is recovered. The solid line shows the path of the aGDA algorithm while the dashed line depicts a possible dynamical annealing trajectory. In this drawing, the "megabasin" containing a low-energy, misfolded conformation has a large associated volume and dominates the severely smoothed potential, causing the aGDA algorithm to locate the misfolded conformation. The dynamical annealing trajectory is also initially in the left megabasin of the smoothed potential. However, eventually, due to the inherent randomness in the dynamics, it is able to cross to the native minimum of lowest energy. This drawing demonstrates the importance of using a smoothing method or boundary potential which biases the initial minimum to the region of the native megabasin. A better boundary potential or smoothing might shift the minimum of the uppermost curve to the right and the aGDA algorithm would succeed.

An analysis of the correlation of the optimization results with the energy gap was performed for the 22-mer discussed above with sequence $(LB)_5N_2$ $(LB)_5$ whose global energy minimum configuration is a β-turn. In this configuration the two linear strands have alternating L and B residues, and the low energy comes from matching the pairwise interactions of hydrophobic B residues on the inside of the turn while keeping the hydrophilic L residues separated and facing away from the core. The density of local minimum $\omega_{min}(E)$ is shown in Figure 13a. Clearly, there is a global energy minimum ($E_0 = -2.339$) configuration which is close to another minimum which has native-like structure ($E_1 = -2.111$). However, each configuration has the correct β-turn conformation of the global minimum native state. Note that we do not necessarily expect to find a gap between the global minimum and *all* other minima.[14,46] The native state of the model protein is expected to consists of a number of substates as has been implied from experimental data[47] and shown unambiguously in analyses of equilibrium molecular dynamics simulations of large peptides and proteins.[48,49] Locating any of these minima corresponds to folding the model. For this model, we find that the third lowest minimum of energy ($E_2 = -1.500$) represents the first minimum outside of the Tier 0 basin (for which this model contains two conformations). The effective energy separation between the native-like and non-native configurations is then $\Delta E_{NN} = E_2 - E_0 = 0.839$, which is significant for this model. The root-mean-square (rms) difference between configurations 0 and 1 is rms(0,1) = 0.266 while rms(0,2) = 0.477 and rms(1,2) = 0.489 supporting this conclusion. Of course, this cutoff is arbitrary. However, we find that configurations with rms differences greater than 0.4 tend to require significant rearrangement and reopening to interconvert.

A second 22-mer with sequence B_9 N_3 $(LB)_5$ was studied. This model is similar to the 22-mer studied above except that a branch of alternating L and B residues was replaced by a homopolymer chain of all hydrophobic B residues. We had less success folding this model using any of the optimization methods applied in this study. The density shown in Figure 13a shows a significant density of local minima at low energies. While we may have found the global minimum for this model, the GPP-based Fokker–Planck dynamics localized 80% of the time in the next to lowest known energy for the model which was found by an intensive MD run with quenches from many high-energy configurations. These results imply that many quite different conformations of similarly low energy can be found. This property is shared by homopolymers, such as the B_{22} model whose $\omega_{min}(E)$ is shown in Figure 13a. For B_{22} the dihedral angle potential is taken to be that of sequence $B_9N_3(LB)_5$. In fact, it appears that the density of local minima for this hybrid model can be almost linearly decomposed into a lobe with homopolymer-like character, as in B_{22}, and another with heteropolymer-like character, as in $(LB)_5N_2(LB)_5$.

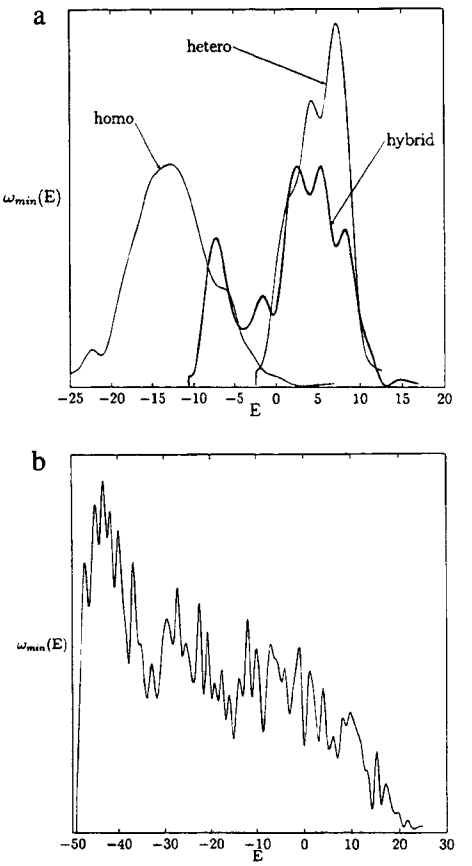

Figure 13. A measure of the density of states of local minima $\omega_{min}(E)$ computed for the 22-mer proteins: (a) the heterosequence $(LB)_5N_2(LB)_5$, the hybrid 22-mer $B_9N_3(LB)_5$, and the homosequence B_{22} (using the torsion potential of the hybrid sequence) and (b) the 46-mer $B_9N_3(LB)_4N_3B_9N_3(LB)_5$ L.

For the $B_9N_3(LB)_5$ model we find a global minimum of ($E_0 = -10.632$) and a number of other close minima ($E_1 = -10.288$, $E_2 = -10.259$, $E_3 = -10.103$, and $E_4 = -9.92$). However, the rms differences between any two of these configurations is significantly greater than that found between the global and second lowest energy minimum in the 22-mer discussed above and analyzed in detail in this work. For example, the differences are rms(0,1) = 0.610, rms(0,2) = 0.466, rms(0,3) = 0.588, and rms(0,4) = 0.528. It would seem that all of these configurations are rather different from one another, meaning that there are a number of low-energy configurations which we can call non-native which are close in energy to the

global energy minimum for this model. The separation in energy is only $\Delta E_{NN} = 0.344$. This small gap correlates well with the poor performances of the GPP-based Fokker–Planck algorithm which located minimum E_2 80% of the time and did not find the lowest known energy minimum for this model. This is true in spite of the fact that the characteristic temperatures T_θ and T_f appear to be similar in this sequence and the heteropolymer sequence $(LB)_5N_2(LB)_5$ for which ΔE_{NN} is significantly larger. We believe that this model, as seen in the density of local minima, has significant homopolymer character, making the energy gap small and making it difficult to isolate the global energy minimum consistently.

In Figure 13b a sample of the local minima distribution for the 46-mer $B_9N_3(LB)_4N_3\ B_9N_3(LB)_5L$ is shown. Note that this molecule, whose density of states was discussed in greater detail previously,[14] has a large number of local minima at low energy approaching the global energy minimum. However, the first non-native state is found at an energy of $\Delta E_{NN} = 3.3$ above the lowest energy minimum,[14] meaning the effective energy gap between native and non-native minima is quite large relative to the folding temperature found[27] and the gap in the 22-mers studied here. This helps to explain the success of the optimization methods for this sequence. Again, we believe this model to be successfully folded if any of these lower energy, compact, native-like states are found.

V. Summary and Conclusions

We find that for the 22-mer used in our comparative study the aGDA and DEM algorithms, which we interpret as being based on a simulated annealing in temperature, are highly successful in locating the lowest energy minimum. We find that the particular sequence used leads to a potential energy hypersurface with a small density of low-energy local minima and that these minima are all associated with a class of native-like states having the same fold as the lowest energy "native" state. Other sequences have a jumble of non-native local energy minima at the lower end of the energy spectrum (with homopolymer character). For these sequences, there is no significant energy gap separating the non-native states from the native and native-like states, and the models do not consistently fold with any of the algorithms studied. As was demonstrated earlier,[14] the 46-mer studied has the desirable property of a significant energy region of native-like folds before the first non-native, minimum-energy compact state appears. This correlates well with the success of the phase space dynamical annealing algorithms on this problem.

Our data indicate that a significant gap between the native-like and non-native states ΔE_{NN} is necessary for the success of any of the algorithms we have studied. This is easily understood as a condition for thermodynamic stability and dominance. This has been discussed in detail before in the context of protein folding (see Introduction) as well as atomic clusters.[8] However, we have no rigorous argument which says that a significant ΔE_{NN} is sufficient for our algorithms to be successful. Thirumalai has proposed that the folding time for a given molecule scales as the cube of the ratio $(T_\theta - T_f)/T_\theta$.[50] We have shown elsewhere that a general property of the GPP-based algorithms is to lower T_θ below the exact thermodynamic value valid for MD simulation. Therefore, if $T_\theta^{GPP} < T_\theta^{MD}$, and if T_f is relatively unaffected (the packet widths in the compact state being narrower), we expect that the folding time for the approximate dynamics will be less than that of the exact dynamics. In fact, this suggests that minimizing the ratio $(T_\theta - T_f)/T_\theta$ may be a criterion not only for sequence optimization but also for the development of optimization algorithms for protein folding.

For the molecules studied, the dynamical annealing algorithm derived from GPP-based Fokker–Planck dynamics is significantly more successful than either the MD simulated annealing or the thermodynamic annealing algorithms such as the aGDA and DEM methods. Perhaps in the application of the aGDA and similar algorithms it will prove important to use a high-temperature dynamics to identify a set of topological superbasins which represent subsets of conformational space, all points of which drain to minimum-energy compact states of a specific fold topology. Our previous analysis supports this conclusion. The aGDA and DEM algorithms are effectively steepest descent algorithms on an evolving effective potential. Therefore, the initial conditions are extremely important, and the boundary potential must be chosen carefully. The importance of the choice of boundary conditions for these algorithms has been recognized and discussed in some detail.[3,6] More work in this area is needed. It is certainly true that the dynamical annealing algorithms have a greater ability to move between basins and, if necessary, correct an early, wrong turn.

The differences in the results for the 22-mer and 46-mer are informative. The GPP-based Fokker–Planck algorithm had the most consistent success. In the case of the 22-mer it was effective in finding the lowest energy native state in spite of the relatively small energy separation ΔE_{NN} between the native and non-native-like states. Small separations correlate well with difficulty in molecular optimization problems.[3,8] In this case of a simple fold topology—the β-turn—the aGDA and DEM algorithms were highly effective. The results for these algorithms were relatively insensitive to the boundary condition chosen. However, in the 46-mer the more complex fold topology made the task of the aGDA algorithm significantly more difficult. We were unable to find an optimal boundary condition which led to a successful annealing. However, the dynamical annealing algorithms—the GPP-based Fokker–Planck method as well as the MD-based annealing—were successful in evolving during the annealing process to recognize the correct lowest energy fold topology. The GPP-based Fokker–Planck annealing method was effective in further isolating a low energy native-like structure while the MD annealing was often caught on a high-energy local minimum.

In this study, we have analyzed these methods as optimization algorithms where the end points are of greatest interest. However, the dynamics and thermodynamics along the annealing trajectories are physically reasonable and, for the methods based on approximate density distributions, show good agreement with exact MD results. Therefore, it might be of interest to further explore the dynamics of folding using these approximate algorithms by simulating the system below the folding temperature without annealing.

Acknowledgment. J.E.S. recognizes the generous support of the donors of the Petroleum Research Fund and the National Science Foundation (CHE-9306375).

Appendix. Derivation of $\langle V \rangle$ and Its First and Second Derivatives

To obtain the equations of motion for the parameters of each packet, we must evaluate the average potential $\langle V \rangle$. We are faced with the usual dilemma that the nonbonded potential is most easily evaluated in Cartesian coordinates while the internal energy terms are most simple in internal coordinates. We evaluate $\langle V \rangle$ in Cartesian coordinates since our wave packet has a simple form in that coordinate system. Our nonbonded empirical potential function for the model protein is pairwise additive so that $V(\mathbf{r}) = V(|\mathbf{r}_i - \mathbf{r}_j|)$, and the effective potential can be written as

TABLE 2: Gaussian Fitting Parameters for the Three Forms of Nonbonded Potential Used in the Model Protein where $V(r) = \sum_k a_k \exp(-b_k r^2/2)$

$4\epsilon[(\sigma/r)^{12} - (\sigma/r)^6]$		$(8\epsilon/3)[(\sigma/r)^{12} + (\sigma/r)^6]$		$4\epsilon(\sigma/r)^{12}$	
a_k	b_k	a_k	b_k	a_k	b_k
3276.338	15.118 77	1.388 467	1.567 669	2792.705	14.459 13
128988.0	27.405 91	37.538 32	4.964 220	85547.84	25.635 37
−0.4556227	1.060 575	1269.092	11.678 86	74.57018	7.6886 37
−8.921689	3.457 895	50779.91	22.920 64	0.8173532	3.4187 81

$$\langle V\rangle = \int d\mathbf{r}_i \int d\mathbf{r}_j \int d\mathbf{p}_i \int d\mathbf{p}_j\, \varrho_i(\mathbf{r}_i,\mathbf{p}_i)\, \varrho_j(\mathbf{r}_j,\mathbf{p}_j)\, V(|\mathbf{r}_i - \mathbf{r}_j|)$$

where $\varrho_i(\mathbf{r}_i)$ and $\varrho_j(\mathbf{r}_j)$ are the density distributions for the ith and jth sites.

First let us consider the nonbonded potential which is fit to a series of Gaussian functions. For a single Gaussian potential $V(\mathbf{r}) = \exp(-\lambda(\mathbf{r} - \mathbf{r}_m)^2/2)$, the average potential and its derivatives are

$$\langle V\rangle = \left(\frac{\hat{\lambda}}{\lambda}\right)^{d/2} \exp\left[-\frac{1}{2}\hat{\lambda}(\mathbf{r}_0 - \mathbf{r}_m)^2\right]$$

$$\nabla_{\mathbf{r}_0}\langle V\rangle = -\hat{\lambda}(\mathbf{r}_0 - \mathbf{r}_m)\langle V\rangle$$

$$\nabla_{\mathbf{r}_0}{}^2\langle V\rangle = \hat{\lambda}[\hat{\lambda}(\mathbf{r}_0 - \mathbf{r}_m)^2 - d]\langle V\rangle$$

where $\hat{\lambda} = \lambda/(1 + \lambda M_{2,0}/d)$. For the three-letter code model, we represent the nonbonded potential by a sum of four Gaussians of the form $V(r) = \sum_k a_k e^{-b_k r^2/2}$. The sets of constants for each of the three potential forms are given in Table 2.

For the confining potential of the form $V_{conf} = (\kappa/2)\sum_i(\mathbf{r}_i - \mathbf{r}_{com})^2$ the effective potential and its derivatives are

$$\langle V\rangle_{conf} = (\kappa/2)\sum_i[(\mathbf{r}_{0,i} - \mathbf{r}_{com})^2 + M_{2,0}(i)]$$

$$\nabla_{r_{0,i}}\langle V\rangle = \kappa(\mathbf{r}_{0,i} - \mathbf{r}_{com})$$

$$\nabla_{r_{0,i}}{}^2\langle V\rangle = \kappa d$$

This form of confining potential was used throughout our study to bias, but not limit, the search to the set of compact configurations.

We explored the use of an alternative confining potential of the form $V_{conf} = (\kappa/2)(R_g{}^2 - R_{g,0}{}^2)^2$ where $R_g{}^2 = (1/N)\sum_i(\mathbf{r}_i - \mathbf{r}_{com})^2$ and $R_{g,0}$ is the radius of gyration of the native state (or global minimum). The average potential and its derivatives are

$$\langle V\rangle_{conf} = \frac{\kappa}{2N^2}\left(\sum_i\left[(\mathbf{r}_{0,i} - \mathbf{r}_{com})^4 + 6M_{2,0}(\mathbf{r}_{0,i} - \mathbf{r}_{com})^2 + \frac{5}{3}M_{2,0}(i) + \sum_{j\neq i}[(\mathbf{r}_{0,i} - \mathbf{r}_{com})^2 + M_{2,0}(i)][(\mathbf{r}_{0,j} - \mathbf{r}_{com})^2 + M_{2,0}(j)] - 2NR_{g,0}{}^2[(\mathbf{r}_{0,i} - \mathbf{r}_{com})^2 + M_{2,0}(i)]\right] + N^2R_{g,0}{}^4\right)$$

$$\nabla_{r_{0,i}}\langle V\rangle = \frac{\kappa}{2N^2}(4(\mathbf{r}_{0,i} - \mathbf{r}_{com})^2 + 12M_{2,0}(i) + 4\sum_{j\neq i}[(\mathbf{r}_{0,j} - \mathbf{r}_{com})^2 + M_{2,0}(j)] - 4NR_{g,0}{}^2)(\mathbf{r}_{0,i} - \mathbf{r}_{com})$$

$$\nabla_{r_{0,i}}{}^2\langle V\rangle = \frac{\kappa}{2N^2}(20(\mathbf{r}_{0,i} - \mathbf{r}_{com})^2 + 36M_{2,0}(i) + 12\sum_{j\neq i}[(\mathbf{r}_{0,j} - \mathbf{r}_{com})^2 + M_{2,0}(j)] - 12NR_{g,0}{}^2)$$

The motivation for using this form of the potential is that the gyration radius of the folded state of a protein can be experimentally determined using light scattering. Thus, $R_{g,0}$ is additional information about the native state, and it was thought that a confining potential of this form could be helpful in biasing the search to the set of configurations with the correct value of gyration radius. For the 22-mer the two forms of confining potential worked similarly. However, our experience was that the constraint about the center-of-mass was less intrusive and led to better results in applications of the optimization algorithm to the 46-mer.

References and Notes

(1) Gibson, K. D.; Scheraga, H. A. In Sarma, M. H., Sarma, R. H., Eds. *Structure and Expression: From Proteins to Ribosomes*; Adenine Press: Schenectady, NY, 1988; Vol. 1.

(2) See: Scheraga, H. A. *Rev. Comput. Chem.* **1992**, *3*, 73; *Theor. Biochem. Mol. Biophys.* **1991**, *2*, 231; *Chem. Scr.* **1989**, *29A*, 3.

(3) Straub, J. E. In Elber, R., Ed. *New Developments in Theoretical Studies of Proteins*; World Scientific: Singapore, 1995.

(4) Kirkpatrick, S.; Gelatt, C. D., Jr.; Vecchi, M. P. *Science* **1983**, *220*, 671.

(5) Stillinger, F. H.; Weber, T. *J. Stat. Phys.* **1988**, *52*, 1429. Head-Gordon, T.; Stillinger, F. H. *Biopolymers* **1993**, *33*, 293.

(6) Piela, L.; Kostrowicki, J.; Scheraga, H. A. *J. Phys. Chem.* **1989**, *93*, 3339.

(7) Ma, J.; Hsu, D.; Straub, J. E. *J. Chem. Phys.* **1993**, *99*, 4024.

(8) Ma, J.; Straub, J. E. *J. Chem. Phys.* **1994**, *101*, 533.

(9) Bryngelson, J. D.; Wolynes, P. G. *Biopolymers* **1990**, *30*, 177; *Proc. Natl. Acad. Sci. U.S.A.* **1987**, *84*, 7524.

(10) Garel, T.; Orland, H. *Europhys. Lett.* **1988**, *6*, 307.

(11) Shakhnovich, E.; Gutin, A. *Biophys. Chem.* **1989**, *34*, 187.

(12) Miller, R.; Danko, C. A.; Fasolka, J.; Balasz, A. C.; Chan, H. S.; Dill, K. A. *J. Chem. Phys.* **1992**, *96*, 768.

(13) Leopold, P. E.; Montal, M.; Onuchic, J. N. *Proc. Natl. Acad. Sci. U.S.A.* **1992**, *89*, 8721.

(14) Honeycutt, J. D.; Thirumalai, D. *Biopolymers* **1992**, *32*, 695. Honeycutt, J. D.; Thirumalai, D. *Proc. Natl. Acad. Sci. U.S.A.* **1990**, *87*, 3526.

(15) Camacho, C.; Thirumalai, D. *Proc. Natl. Acad. Sci. U.S.A.* **1993**, *90*, 6369. Camacho, C.; Thirumalai, D. *Phys. Rev. Lett.* **1993**, *71*, 2505.

(16) Chan, H. S.; Dill, K. A. *J. Chem. Phys.* **1993**, *99*, 2116; **1994**, *100*, 9238.

(17) Socci, N.; Onuchic, J. *J. Chem. Phys.* **1994**, *101*, 1519.

(18) Sali, A.; Shakhnovich, E. I.; Karplus, M. *J. Mol. Biol.* **1994**, *235*, 1614.

(19) Sali, A.; Shakhnovich, E. I.; Karplus, M. *Nature* **1994**, *369*, 248.

(20) Flory, P. J. *Principles of Polymer Chemistry*; Cornell University Press: Ithaca, NY, 1953.

(21) Lifshitz, I. M.; Grosberg, A. Yu.; Khokhlov, A. R. *Rev. Mod. Phys.* **1978**, *50*, 683.

(22) de Gennes, P. G. *Scaling Concepts in Polymer Physics*; Cornell University Press: Ithaca, NY, 1979.

(23) Grosberg, A. Yu.; Nechaev, S. K.; Shakhnovich, E. I. *J. Phys. (Paris)* **1988**, *49*, 2095.

(24) Ma, J.; Straub, J. E.; Shakhnovich, E. *J. Chem. Phys.* **1995**, *103*, 2615.

(25) Chan, H. S.; Dill, K. A. *Annu. Rev. Biophys. Biophys. Chem.* **1991**, *20*, 447.

(26) A recent review of theoretical approaches to the protein folding problem is given by: Karplus, M.; Shakhnovich, E. In *Protein Folding*; Creighton, T., Ed.; Freeman: San Francisco, 1992.

(27) Guo, Z.; Thirumalai, D. *Biopolymers* **1994**, *35*, 137.

(28) Shakhnovich, E. I.; Gutin, A. M. *Proc. Natl. Acad. Sci. U.S.A.* **1993**, *90*, 7195.
(29) Shakhnovich, E. *Biochemistry* **1994**, *33*, 10026.
(30) Frauenfelder, H.; Wolynes, P. G. *Phys. Today* **1994** (Feb), 58.
(31) Guo, Z.; Thirumalai, D.; Honeycutt, J. D. *J. Chem. Phys.* **1992**, *97*, 525.
(32) Straub, J. E.; Amara, P.; Ma, J. *J. Chem. Phys.* **1995**, *103*, 1574.
(33) Aarts, E.; Korst, J. *Simulated Annealing and Boltzmann Machines*; Wiley: New York, 1990.
(34) Gardiner, C. W. *Handbook of Stochastic Methods*; Springer-Verlag: Berlin, 1983.
(35) Risken, H. *The Fokker-Planck Equation: Methods of Solution and Applications*; Springer-Verlag: Berlin, 1989.
(36) Amara, P.; Hsu, D.; Straub, J. E. *J. Phys. Chem.* **1993**, *97*, 6715.
(37) Tsoo, C.; Brooks III, C. L. *J. Chem. Phys.* **1994**, *101*, 6405.
(38) Rey, J.; Skolnick, J. *J. Chem. Phys.* **1991**, *158*, 199.
(39) The classical trajectory-bundle TDSCF method provides greater flexibility than Gaussian wave packets at the cost of introducing more degrees of freedom. See: Gerber, R. B.; Ratner, M. A. *Adv. Chem. Phys.* **1988**, *70*, 97. Schatz, G. C.; Buch, V.; Ratner, M. A.; Gerber, R. B. *J. Chem. Phys.* **1983**, *79*, 1808. Buch, V.; Gerber, R. B.; Ratner, M. A. *Chem. Phys. Lett.* **1983**, *101*, 44. Gerber, R. B.; Buch, V.; Ratner, M. A. *J. Chem. Phys.* **1982**, *77*, 3022; *Chem. Phys. Lett.* **1982**, *91*, 173.
(40) Brooks, C. L.; Karplus, M.; Pettitt, M. *Proteins: A Theoretical Perspective of Dynamics, Structure, and Thermodynamics*; John Wiley and Sons: New York, 1988.
(41) Némethy, G.; Gibson, K. D.; Palmer, K. A.; Yoon, C. N.; Paterlini, G.; Zagari, A.; Rumsey, S.; Scheraga, H. A. *J. Phys. Chem.* **1992**, *96*, 6472. Roterman, I. K.; Lambert, M. H.; Gibson, K. D.; Scheraga, H. A. *J. Biomol. Struct. Dyn.* **1989**, *7*, 421.
(42) Garrett, D. G.; Kastella, K.; Ferguson, D. M. *J. Am. Chem. Soc.* **1992**, *114*, 6555.
(43) Sippl, M. *J. Mol. Biol.* **1990**, *213*, 859 (see also: Godzik, A.; Kolinski, A.; Skolnick, J. *J. Mol. Biol.* **1992**, *227*, 227.
(44) Allen, M. P.; Tildesley, D. J. *Computer Simulation of Liquids*; Oxford: Bristol, 1990.
(45) Orešič, M.; Shalloway, D. *J. Chem. Phys.* **1994**, *101*, 9844.
(46) Abkevich, V. I.; Gutin, A. M.; Shakhnovich, E. I. *J. Chem. Phys.* **1994**, *101*, 6052.
(47) Frauenfelder, H.; Sligar, S. G.; Wolynes, P. G. *Science* **1991**, *254*, 1598. Frauenfelder, H.; Parak, F.; Young, R. D. *Annu. Rev. Biophys. Chem.* **1988**, *17*, 451.
(48) Elber, R.; Karplus, M. *Science* **1987**, *235*, 318.
(49) Straub, J. E.; Thirumalai, D. *Proc. Natl. Acad. Sci. U.S.A.* **1993**, *90*, 809. Straub, J. E.; Thirumalai, D. *Proteins* **1993**, *15*, 360. Straub, J. E.; Rashkin, A.; Thirumalai, D. *J. Am. Chem. Soc.* **1994**, *116*, 2049.
(50) Thirumalai, D. *J. Phys. (Paris)*, in press.

JP950773N